Size effects on excitons in nano-rings

2000 J. Phys.: Condens. Matter 12 9145

(http://iopscience.iop.org/0953-8984/12/43/304)

J. Phys.: Condens. Matter **12** (2000) 9145–9151. Printed in the UK PII: S0953-8984(00)16940-1

Size effects on excitons in nano-rings

Hui Hu†, Dai-Jun Li†, Jia-Lin Zhu†‡ and Jia-Jiong Xiong†

† Department of Physics, Tsinghua University, Beijing 100084, People's Republic of China
‡ Centre for Advanced Study, Tsinghua University, Beijing 100084, People's Republic of China

Received 7 September 2000

Abstract. The size effects on an exciton in a nano-ring are investigated theoretically by using an effective-mass Hamiltonian which can be separated into terms in centre-of-mass and relative coordinates. The binding energy and oscillator strength of the ground state are calculated for two different ring radii as functions of the ring width. The resulting linear optical susceptibility of the low-lying exciton states is also discussed.

Recent progress in nanofabrication techniques has made it possible to construct self-assembled InGaAs nano-rings [1–5]. Quite unlike the previously fabricated sub-micron GaAs quantum rings [6], the nano-rings now achieved are so small (with characteristic inner/outer radius of 20/100 nm and 2–3 nm in height) that the electrons and holes can propagate coherently (non-diffusively) throughout the ring. In view of this, nano-rings can be viewed as promising candidates for application in microelectronics as well as conventional quantum dots. Moreover, the additional non-simply connected geometry of nano-rings is of inherent interest at the moment [7–11].

While the conventional quantum dots have been investigated theoretically and experimentally in depth [12–16], nano-rings with strong quantum effects have only been treated recently [9, 11, 17–23]. In particular, theoretical results related to the quantum confinement effects on *exciton* states in nano-rings are very rare. Only recently did Song and Ulloa report numerical calculations of the binding energy and electron–hole separation of the exciton in an external magnetic field [11]. They claim that the excitons in nano-rings behave to a great extent as those in quantum dots of similar dimensions.

In this paper, we would like to investigate the size effects on excitons in nano-rings by introducing a simplified confining potential, which is applicable to the *realistic* self-assembled semiconducting InGaAs nano-rings achieved to date [2, 4, 5]. To explore the role of different confinements, we express the model Hamiltonian in terms of the centre-of-mass and relative coordinates and calculate binding energies, oscillator strengths and their dependence on the nano-ring width, as well as the linear optical susceptibility which would be measurable in photoluminescence experiments, for example.

Our model is a two-dimensional exciton in a nano-ring, simulating recent experimental nano-ring structures [2, 4, 5]. The nano-ring is described by an electron–hole pair ($i = \mathrm{e}, \mathrm{h}$) with an effective band-edge mass m_i^* moving in an x–y plane, and a ring-like confining potential is introduced as

$$U(\vec{r}_i) = \frac{1}{2R_0^2} m_i^* \omega_i^2 (\vec{r}_i^{\,2} - R_0^2)^2$$

0953-8984/00/439145+07$30.00

where R_0 is the radius of the ring and ω_i is the characteristic frequency of the radial confinement, giving a characteristic ring width

$$W \approx 2\sqrt{\frac{\hbar}{2m_i^*\omega_i}}$$

for each particle. The resulting model Hamiltonian is thus given by

$$\mathcal{H} = \sum_{i=\mathrm{e,h}} \left[\frac{\vec{p}_i^{\,2}}{2m_i^*} + U(\vec{r}_i) \right] - \frac{e^2}{4\pi\varepsilon_0\varepsilon_r|\vec{r}_\mathrm{e} - \vec{r}_\mathrm{h}|} \tag{1}$$

where $\vec{r}_i = (x_i, y_i)$ and $\vec{p}_i = -\mathrm{i}\hbar\vec{\nabla}_i$ denote the position vector and momentum operator, ε_0 is the vacuum permittivity and ε_r is the static dielectric constant of the host semiconductor. It should be pointed out that the present ring-like confining potential can be rewritten as

$$U(\vec{r}_i) = \frac{1}{2}m_i^*\omega_i^2(r_i - R_0)^2\frac{(r_i + R_0)^2}{R_0^2}.$$

If one replaces the operator r_i in the factor $(r_i + R_0)^2/R_0^2$ by its mean value $\langle r_i\rangle = R_0$, the confining potential returns to the widely used parabolic form [2, 11, 20, 22]. On the other hand, for narrow rings (with steep confinement) our confining potential gives a more realistic description than does the parabolic form. In the latter, as pointed out by Song and Ulloa [11], the associated wavefunctions fail in a real system because the increased confinement may push the levels into the anharmonic part of the potential and even produce deconfinement of carriers. Figures 1(a) and 1(b) display the shape of the ring potential with two different radii: 10 and 30 nm. The solid and dashed lines correspond to the ring widths $W = 16.7$ and 9.6 nm, respectively.

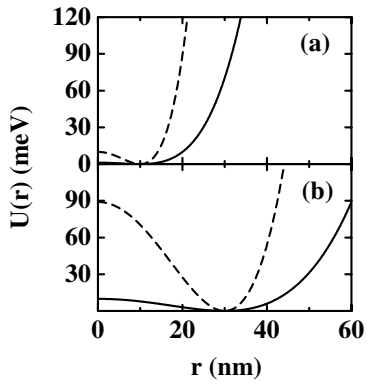

Figure 1. The confining potential $U(\vec{r}) = [m_\mathrm{e}^*\omega_\mathrm{e}^2/(2R_0^2)](\vec{r}^{\,2} - R_0^2)^2$ with different ring radii R_0: 10 nm (a) and 30 nm (b). The solid and dashed lines correspond to the ring widths $W = 16.7$ and 9.6 nm, respectively.

In terms of the relative coordinate $\vec{r} = \vec{r}_\mathrm{e} - \vec{r}_\mathrm{h}$ and centre-of-mass coordinate

$$\vec{R} = \frac{m_\mathrm{e}^*\vec{r}_\mathrm{e} + m_\mathrm{h}^*\vec{r}_\mathrm{h}}{m_\mathrm{e}^* + m_\mathrm{h}^*}$$

the model Hamiltonian is divided into

$$H = \mathcal{H}_{cm}(\vec{\boldsymbol{R}}) + \mathcal{H}_{rel}(\vec{r}) + \mathcal{H}_{mix}(\vec{\boldsymbol{R}}, \vec{r})$$

$$H_{cm} = \frac{\vec{\boldsymbol{P}}_{cm}^2}{2M} + \frac{M\omega_{cm}^2}{2R_0^2}(\vec{\boldsymbol{R}}^2 - R_0^2)^2$$

$$H_{rel} = \frac{\vec{p}_{rel}^2}{2\mu} + \frac{\mu}{2}\frac{(m_{\rm h}^{*3}\omega_{\rm e}^2 + m_{\rm e}^{*3}\omega_{\rm h}^2)}{M^3R_0^2}r^4 - \mu\omega_{rel}^2 r^2 - \frac{e^2}{4\pi\varepsilon_0\varepsilon_r r} \tag{2}$$

$$H_{mix} = -2\mu(\omega_{\rm e}^2 - \omega_{\rm h}^2)(\vec{\boldsymbol{R}}\cdot\vec{r} - \frac{\vec{\boldsymbol{R}}^3\cdot\vec{r}}{R_0^2}) + \frac{\mu\omega_{rel}^2}{R_0^2}\left[R^2r^2 + 2(\vec{\boldsymbol{R}}\cdot\vec{r})^2\right] + 2\mu\frac{(m_{\rm h}^{*2}\omega_{\rm e}^2 - m_{\rm e}^{*2}\omega_{\rm h}^2)}{M^2R_0^2}\vec{\boldsymbol{R}}\cdot\vec{r}^3$$

where $\mu = m_{\rm e}^* m_{\rm h}^*/M$ is the electron–hole reduced mass and $M = m_{\rm e}^* + m_{\rm h}^*$ is the total mass. We have also introduced a centre-of-mass frequency

$$\omega_{cm} = \sqrt{\frac{m_{\rm e}^*\omega_{\rm e}^2 + m_{\rm h}^*\omega_{\rm h}^2}{M}}$$

and a relative frequency

$$\omega_{rel} = \sqrt{\frac{m_{\rm h}^*\omega_{\rm e}^2 + m_{\rm e}^*\omega_{\rm h}^2}{M}}.$$

The main purpose of the above change of variable is to use the solutions of H_{cm} and H_{rel} as a basis for solving the full Hamiltonian. Those solutions, i.e. those labelled as $\psi_\lambda^{cm}(\vec{\boldsymbol{R}})$ and $\psi_{\lambda'}^{rel}(\vec{r})$, can be solved by the series expansion method [24, 25]. Here, $\lambda = \{n_{cm}, l_{cm}\}$ and $\lambda' = \{n_{rel}, l_{rel}\}$ represent the quantum number pair of the radial quantum number n and orbital angular momentum quantum number l. Another advantage coming from centre-of-mass and relative coordinate separation is that we can include the negative Coulomb interaction $-e^2/(4\pi\varepsilon_0\varepsilon_r r)$ in H_{rel}, thus avoiding the well-known poor convergence of the parabolic basis when the characteristic system scale is beyond the effective Bohr radius [11, 26]. We now search for the wavefunctions of the exciton in the form

$$\Psi = \sum_{\lambda,\lambda'} A_{\lambda,\lambda'}\psi_\lambda^{cm}(\vec{\boldsymbol{R}})\psi_{\lambda'}^{rel}(\vec{r}). \tag{3}$$

Due to the cylindrical symmetry of the problem, the exciton wavefunctions can be labelled by the total orbital angular momentum $L = l_{cm} + l_{rel}$. To obtain the coefficients $A_{\lambda,\lambda'}$, the total Hamiltonian is diagonalized in the space spanned by the product states $\psi_\lambda^{cm}(\vec{\boldsymbol{R}})\psi_{\lambda'}^{rel}(\vec{r})$. In the present calculations, we first solve the single-particle problem of centre-of-mass and relative Hamiltonians H_{cm} and H_{rel}, keep several hundreds of the single-particle states and then pick up the low-lying energy levels to construct several thousands of product states. Note that our numerical diagonalization scheme is very efficient and essentially exact in the sense that the accuracy can be improved as required by increasing the total number of selected product states.

Once the coefficients $A_{\lambda,\lambda'}$ are obtained, one can calculate directly the measurable properties, such as the linear optical susceptibility of the nano-rings, whose imaginary part is related to the absorption intensity measured by optical emission experiments. In theory, the linear optical susceptibility is proportional to the dipole matrix elements connecting one electron–hole pair state m and the vacuum state, which in turn is proportional to the oscillator strengths F_m. In the dipole approximation, it is given by [12, 26, 27]

$$F_m = \left|\int\int \mathrm{d}\vec{\boldsymbol{R}}\,\mathrm{d}\vec{r}\;\Psi(\vec{\boldsymbol{R}}, \vec{r})\delta(\vec{r})\right|^2 = \left|\sum_{\lambda,\lambda'} A_{\lambda,\lambda'}\psi_{\lambda'}^{rel}(\boldsymbol{0})\int \mathrm{d}\vec{\boldsymbol{R}}\;\psi_\lambda^{cm}(\vec{\boldsymbol{R}})\right|^2 \tag{4}$$

where the factor $\psi_{\lambda'}^{rel}(\mathbf{0})$ and the integral over $\vec{\boldsymbol{R}}$ ensure that only the excitons with $L = 0$ are created by absorbing photons. Therefore, the frequency dependence of the linear optical susceptibility $\chi(\omega)$ can be expressed as [12, 26, 27]

$$\chi(\omega) \propto \sum_m \frac{F_m}{\hbar\omega - E_g - E_m - \mathrm{i}\Gamma} \tag{5}$$

where E_g and E_m are the respective semiconducting band gap of InGaAs and energy levels of the exciton, and Γ has been introduced as a phenomenological broadening parameter.

In what follows we constrain ourselves to the subspace $L = 0$, the most interesting case, throughout the calculations. As an interesting example of a typical system, we have taken the parameters $m_{\mathrm{e}}^* = 0.067m_{\mathrm{e}}$, the effective mass of the heavy hole $m_{\mathrm{h}}^* = 0.335m_{\mathrm{e}}$ (m_{e} is the bare mass of a single electron) and $\varepsilon_r = 12.4$, which are appropriate to InGaAs material [2, 20, 22]. The electron and hole are considered to be confined under the same potential barrier, i.e. $m_{\mathrm{e}}^*\omega_{\mathrm{e}}^2 = m_{\mathrm{h}}^*\omega_{\mathrm{h}}^2$. If we choose the characteristic energy and length scale to be the effective Rydberg $R^* = m_{\mathrm{e}}^* e^4/(2\hbar^2(4\pi\varepsilon_0\varepsilon_r)^2)$ and the effective Bohr radius $a_B^* = 4\pi\varepsilon_0\varepsilon_r\hbar^2/(\mu e^2)$, we find that $R^* = 5.0$ meV and $a_B^* = 11.8$ nm. In the following, we perform the calculations for two ring radii: 10 and 30 nm. The ring width can be tuned by the confining potential; e.g. $W = 10$ nm corresponds to $\hbar\omega_{\mathrm{e}} = 15$ meV.

Figure 2 displays the exciton binding energies obtained for different ring radii: $R_0 = 10$ nm and 30 nm, as functions of the nano-ring width. For comparison, the binding energy of a quantum dot with a parabolic potential $U(\vec{r}) = \frac{1}{2}m^*\omega_0^2 r^2$ is also presented, as a dashed line (for quantum dots, $2W = 2\sqrt{\{\hbar/(m^*\omega_0)\}}$ is the diameter). Notice that $E_b = E_{\mathrm{e-h}}^0 - E_{grnd}^{ex}$, where the first term refers to just the confinement ground state of the electron and hole, ignoring the Coulomb interaction. It is obvious that for relatively large widths, the exciton binding energy for small-radius nano-rings is larger than for the large-radius ones, as expected. This difference is a reflection of the strong quantum confinement in small nano-rings. As the ring width decreases, the binding energy for nano-rings with a large radius increases rapidly. For widths less than $\approx$11 nm, however, the two solid curves cross and their sequence is reversed. This crossover is caused by the strong anisotropic confinement in nano-rings: for smaller ring widths, the resulting exciton wavefunctions are increasingly elongated along the ring, and thus the exciton is confined in a quasi-one-dimensional system with a characteristic size $\approx W$. On

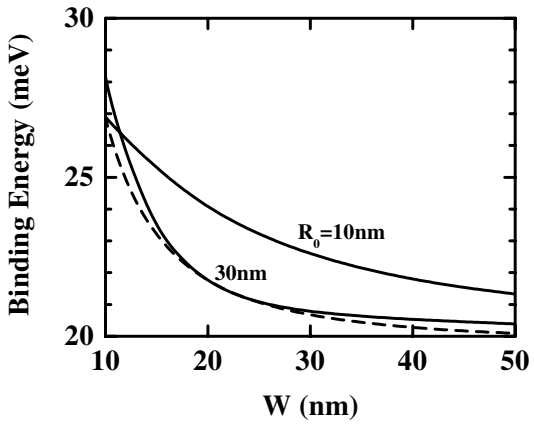

Figure 2. The exciton binding energies for the nano-ring as functions of the ring width for two different ring radii $R_0 = 10$ and 30 nm. For comparison, the result for a parabolic quantum dot is also displayed, as a dashed line.

the other hand, by decreasing the ring radius with a fixed potential strength (or a fixed ring width), nano-rings can be tuned from quasi-one-dimensional to two-dimensional systems. In other words, nano-rings will behave like quantum dots when their radii are comparable to the widths (see figure 1(a)). One can thus expect that with a fixed sufficiently small ring width, the effective size of the exciton might be smaller for a larger ring radius, and in turn cause enhancement of its binding energy.

Another feature shown in figure 2 is the similarity of the curves for the large-radius nano-ring and the quantum dot. This is due to the confinement areas of the two systems being comparable; as pointed out by Song and Ulloa, the excitons in nano-rings behave to a great extent as those in quantum dots of similar dimensions [11]. It is also important to emphasize that for a nano-ring with a large ring radius and ring width, the binding energy approaches approximately the exact result for a free two-dimensional exciton, i.e. $E_b = 4R^* = 20$ meV.

Figure 3 shows the exciton oscillator strengths versus the ring width, for two ring radii (two solid lines) and a quantum dot with a parabolic potential (the dashed line). It is readily seen that the oscillator strength of the large-radius nano-ring is much larger than that of the small-radius nano-ring for the whole range of widths shown, which is also an indication of the strong quantum confinement in small nano-rings, as mentioned above. For a larger ring width, the oscillator strengths of the two nano-rings clearly increase, but not as fast as that of the quantum dot.

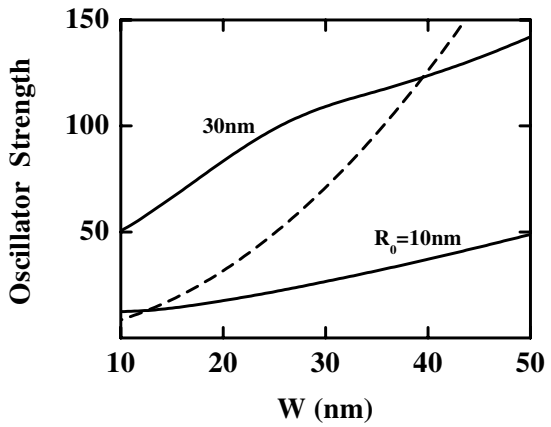

Figure 3. The exciton oscillator strengths versus the ring width, for two ring radii (two solid lines) and a quantum dot with a parabolic potential (the dashed line).

To support the experimental relevance of our results, we have also calculated the linear optical susceptibility of nano-rings. Figures 4(a) and 4(b) show typical results for different values of the ring width and two ring radii, where a broadening parameter $\Gamma = 0.5$ meV is used. Those curves represent all the possible transitions of excitonic states which would be measurable via photoluminescence excitation (PLE) measurements. In contrast to the case for conventional quantum dots, in which the low-lying exciton-state transitions have the same amplitudes and are nearly equally distributed (a reflection of excitations of the centre-of-mass degree of freedom), the low-lying transitions of nano-rings show a rapid damping with frequency and their positions are not periodic. This difference is a refection of the anisotropic confinement of nano-rings: since the exciton is confined in a quasi-one-dimensional system, its centre-of-mass degree of freedom is greatly suppressed and its relative motion becomes dominant; this results in the destruction of the regular patterns observed in quantum dots.

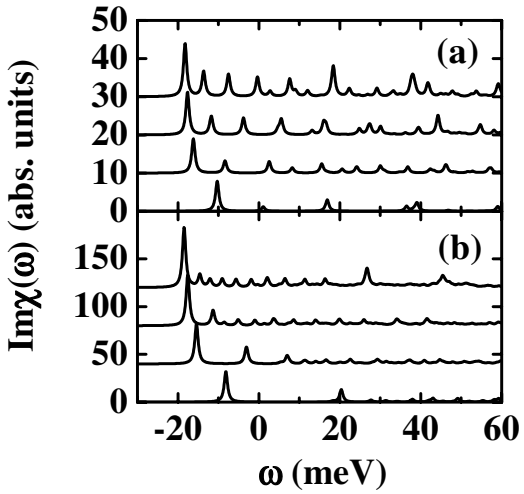

Figure 4. The imaginary part of the linear optical susceptibility as a function of frequency ω for different values of the ring width and two different ring radii $R_0 = 10$ nm (a) and $R_0 = 30$ nm (b). In each panel, from bottom to top, the ring widths are 10, 15, 20 and 25 nm. For clarity, the semiconducting band gap E_g is set to zero.

Note that this behaviour is indeed observed in a recent experiment [3]. Another noticeable feature in figures 4(a) and 4(b) is that those transition peaks are strongly red-shifted as the ring width increases, indicating that there is less confinement for larger ring widths.

In conclusion, we have shown the strong quantum confinement effects on excitons in a nano-ring on the basis of a simple model Hamiltonian. By numerical diagonalization, we calculate the binding energies, oscillator strengths and their dependences on the nano-ring width, as well as the linear optical susceptibility. The anisotropic confinement in nano-rings is clearly demonstrated; this could be confirmed by future measurements of optical emission on InGaAs nano-rings with tunable sizes.

Acknowledgments

The financial support from NSF-China (Grant No 19974019) and China's '973' programme is gratefully acknowledged.

References

[1] Warburton R J, Schäflein C, Haft D, Bickel F, Lorke A, Karrai K, Garcia J M, Schoenfeld W and Petroff P M 2000 *Nature* **405** 926
[2] Lorke A, Luyken R J, Govorov A O, Kotthaus J P, Garcia J M and Petroff P M 2000 *Phys. Rev. Lett.* **84** 2223
[3] Pettersson H, Warburton R J, Lorke A, Karrai K, Kotthaus J P, Garcia J M and Petroff P M 2000 *Physica* E **6** 510
[4] Lorke A and Luyken R J 1998 *Physica* B **256** 424
[5] Lorke A, Luyken R J, Fricke M, Kotthaus J P, Medeiros-Ribeiro G, Garcia J M and Petroff P M 1999 *Microelectron. Eng.* **47** 95
[6] Mailly D, Chapelier C and Benoit A 1993 *Phys. Rev. Lett.* **70** 2020
[7] Wendler L and Fomin V M 1995 *Phys. Rev.* B **51** 17 814
[8] Chaplik A 1995 *JETP Lett.* **62** 900
[9] Halonen V, Pietiläinen P and Chakraborty T 1996 *Europhys. Lett.* **33** 377

[10] Römer R A and Raikh M E 2000 *Phys. Rev.* B **62** 7045
[11] Song J and Ulloa S E 2000 *Preprint* cond-mat/0008407
[12] Que W 1992 *Phys. Rev.* B **45** 11 036
[13] Halonen V, Chakraborty T and Pietiläinen P 1992 *Phys. Rev.* B **45** 5980
[14] Song J and Ulloa S E 1995 *Phys. Rev.* B **52** 9015
[15] Uozumi T, Kayanuma Y, Yamanaka K, Edamatsu K and Itoh T 1999 *Phys. Rev.* B **59** 9826
[16] Jacak L, Hawrylak P and Wójs A 1998 *Quantum Dots* (Berlin: Springer) and references therein
[17] Chakraborty T and Pietiläinen P 1994 *Phys. Rev.* B **50** 8460
[18] Gudmundsson V and Loftsdóttir Á 1994 *Phys. Rev.* B **50** 17 433
[19] Wendler L, Fomin V M, Chaplik A V and Govorov A O 1996 *Phys. Rev.* B **54** 4794
[20] Emperador A, Pi M, Barranco M and Lorke A 2000 *Phys. Rev.* B **62** 4573
[21] Koskinen M, Manninen M, Mottelson B and Reimann S 2000 *Preprint* cond-mat/004095
[22] Hu H, Zhu J-L and Xiong J J 2000 *Preprint* cond-mat/0005520
[23] Borrmann P and Harting J 2000 *Preprint* cond-mat/0008464
[24] Zhu J-L, Xiong J J and Gu B-L 1990 *Phys. Rev.* B **41** 6001
[25] Zhu J-L, Li Z Q, Yu J Z, Ohno K and Kawazoe Y 1997 *Phys. Rev.* B **55** 1
[26] Song J and Ulloa S E 1995 *Phys. Rev.* B **52** 9015
[27] Bryant G W 1988 *Phys. Rev.* B **37** 8763